CASE STUDIES OF WATER VAPOR AND SURFACE LIQUID WATER FROM AVIRIS DATA MEASURED OVER DENVER, CO AND DEATH VALLEY, CA

B.-C. Gao[1], K. S. Kierein-Young[1,2], A. F. H. Goetz[1,2],
E. R. Westwater[3], B. B. Stankov[3], and D. Birkenheuer[4]

[1]CSES/CIRES, Campus Box 449, University of Colorado, Boulder, CO
[2]Department of Geological Sciences, University of Colorado, Boulder, CO
[3]NOAA/ERL/ Wave Propagation Laboratory, Boulder, CO
[4]Cooperative Institute for Research in the Atmosphere (CIRA), Ft. Collins, CO

Abstract. High spatial resolution column atmospheric water vapor amounts and equivalent liquid water thicknesses of surface targets are retrieved from spectral data collected by the Airborne Visible/Infrared Imaging Spectrometer (AVIRIS). The retrievals are made using a nonlinear least squares curve fitting technique. Two case studies from AVIRIS data acquired over Denver-Platteville area, Colorado and over Death Valley, California are presented. The column water vapor values derived from AVIRIS data over the Denver-Platteville area are compared with those obtained from radiosondes, ground level upward-looking microwave radiometers, and geostationary satellite measurements. The column water vapor image shows spatial variation patterns related to the passage of a weather front system. The column water vapor amounts derived from AVIRIS data over Death Valley decrease with increasing surface elevation. The derived liquid water image clearly shows surface drainage patterns.

I. Introduction

Water vapor is one of the most important atmospheric gases. The integrated water vapor content from ground to space has important applications to meteorology, hydrology, climate, and radio interferometry. In this paper, the integrated water vapor content is referred to as column water vapor amount or as precipitable water vapor (PWV). The liquid water content of vegetation is related to the stress conditions of vegetation. Remote sensing of liquid water content of vegetation has important applications to forestry and agriculture. The soil moisture content is important to agriculture, forestry, hydrology, and engineering geology.

Satellite remote sensing of PWV with an accuracy of approximately 10% over the oceans using microwave emission measurements is a proven technique (Alishouse, 1983). However, the variability of land surface microwave emissivities poses difficulties in determining PWV over land from satellite microwave data. Column water vapor retrievals over land from satellite IR emission measurements using, for example, the split window technique (Chesters et al., 1983) are possible during clear conditions.

Recently, there have been several reported successes in remote sensing of column atmospheric water vapor amounts from aircraft measurements of solar radiation reflected by the land surface near 1 μm (Gao and Goetz, 1990; Conel et al., 1989; Frouin et al., 1990). These remote sensing techniques are referred to as optical techniques. Gao and Goetz (1990) have also reported the derivation of moisture content of vegetation using liquid water absorption features near 1 μm.

Column water vapor amounts can be obtained from the ground with upward-looking microwave radiometers (Hogg et al., 1983). The Wave Propagation Laboratory (WPL) of the National Oceanic and Atmospheric Administration (NOAA) operates a limited network of dual-channel microwave radiometers (Westwater and Snider, 1989). Radiometers are now routinely operated at Stapleton International Airport in Denver, Colorado and at Platteville, Colorado (approximately 60 km north of Denver). In order to verify the optical techniques, an experiment was designed. Specifically, the Airborne Visible/Infrared Imaging Spectrometer (AVIRIS) (Vane, 1987) was requested to make measurements over the Denver-Platteville area. Column water vapor amounts were to be retrieved from AVIRIS data and then compared with column water vapor amounts measured with the two microwave radiometers mentioned above. The AVIRIS made the measurements around 19:40 UTC 22 March 1990. At this time, the sky was clear. However, snow started later in the day. The AVIRIS measurements happened to be

conducted in the middle of another experimental project, the Winter Icing and Storm Project (WISP90) (Stankov et al., 1990) conducted by NOAA Forecast Systems Laboratory (FSL) for determining the utility of unattended microwave radiometers in detecting, and providing input to forecasts of aircraft icing. WISP90 collected data from microwave radiometers, infrared radiometers, lidar ceilometers, radio-acoustic sounding systems (RASS), and radiosondes at several locations in Colorado. Also, meteorological parameters were collected from approximately 20 surface stations in Colorado. Meanwhile, data from the Visible Infrared Spin Scan Radiometer (VISSR) Atmospheric Sounder (VAS) on the NOAA Geostational Operational Environmental Satellite (GOES) were collected and archived by NOAA FSL's Program for Regional Observing and Forecasting Services (PROFS). The WISP90 data provided information on the meteorological conditions around the AVIRIS measurements and allowed better interpretation of the AVIRIS and the microwave radiometers data. In this paper, the water vapor measurements with AVIRIS, microwave radiometers, and VAS are compared.

AVIRIS measurements over Death Valley, California were obtained on September 29, 1989 as part of the Geologic Remote Sensing Field Experiment (GRSFE). At the time of the overflight, some surface areas were wet, based on field observations. Measurements of reflectance spectra of samples collected from the field clearly showed liquid water absorption features near 0.98, 1.2, 1.6, and 2.2 μm. Because of the presence of wet surface areas when the AVIRIS measurements were made, we decided to further test the ability of the algorithm (Gao and Goetz, 1990) for simultaneous retrievals of the atmospheric water vapor amount and the surface liquid water content from the AVIRIS data. The results are described in this paper.

II. Imaging Spectrometers: the Optical Technique

Imaging spectrometers acquire images in hundreds of contiguous spectral bands such that for each picture element (pixel) a complete reflectance or emittance spectrum can be derived from the wavelength region covered (Goetz et al., 1985). AVIRIS is now an operational imaging spectrometer. This instrument images the Earth's surface in 224 spectral bands, each approximately 10 nm wide, covering the region 0.4-2.5 μm, from an ER-2 aircraft at an altitude of 20 km. The ground instantaneous field of view is 20 x 20 m^2.

A technique for simultaneous retrievals of atmospheric water vapor amount and surface liquid water content has been described by Gao and Goetz (1990). In this technique, the quantitative retrieval is made by curve fitting AVIRIS spectra with calculated spectra near 1 μm using atmospheric and liquid water transmission models, and a nonlinear least squares fitting technique. Figure 1 shows an example of spectral curve fitting for retrieving water vapor amount only. During the fitting process, the water vapor amount and the spectral background, a linear function of wavelength, are allowed to vary. The best estimates of the water vapor amount and the spectral background are obtained when the sum of the squared differences between the observed and the calculated spectra is minimized. Examples of fitting AVIRIS spectra over wet areas for simultaneous retrievals of atmospheric water vapor and surface liquid water content are presented later in this paper. Our technique is applicable for retrievals from AVIRIS data obtained on clear days with visibilities 20 km or greater. Because atmospheric scattering is not modeled directly, the technique is not applicable for retrievals from AVIRIS data measured on hazy days. Under these circumstances, the scattering effect must be modeled.

III. Results

Column water vapor amounts are retrieved from AVIRIS data measured over the Denver-Platteville area, and both column water vapor amounts and surface liquid water thicknesses are retrieved from AVIRIS data measured over Death Valley using the spectral curve fitting technique.

A. Denver-Platteville, Colorado

Figure 2a shows a 0.86 μm image of the Denver-Platteville area. The AVIRIS radiances were averaged spatially on a 2 x 2 pixel basis when the image was produced. The spatial averaging was necessary because of the limitation of our image processing hardware. The Denver Stapleton International Airport is at the lower left part of the image; Platteville is at the upper part. Highway 85, which connects Denver and Platteville, is seen as a curved line. The image covers a surface area of approximately 11 x 68 km^2.

Column water vapor amounts were retrieved by curve fitting the 0.94-μm water vapor band. The AVIRIS data were averaged spatially on a 4 x 4 pixel basis to decrease the computer time. The retrieval took approximately 25 hours on a Microvax III computer. Low vertical resolution temperature, pressure, and water vapor volume mixing

ratio profiles, measured near the airport by a six-channel microwave radiometer, were used in the spectral calculations during the curve fitting process. Figure 2b shows an image processed from the retrieved column water vapor values. To produce a water vapor image having the same size as the image in Fig. 2a, the retrieved water vapor values were zoomed spatially on a 2 x 2 pixel basis. The narrow vertical bar on the right side of Fig. 2b gives the scale of water vapor values from 0.53 cm (black) to 0.76 cm (white), a very small range. The column water vapor values in the entire scene had a mean of 0.640 cm and a standard deviation of 0.044 cm. Horizontal lines in Fig. 2b are due to small errors in the AVIRIS radiometric calibration. Larger scale features are also obvious in Fig. 2b. From the airport to Platteville, the image shows a dark-bright-dark-bright pattern.

A topographic map of the AVIRIS scene is shown in Fig. 2c. Generally, the surface elevation decreases from the airport area (~1630 m) to Platteville (~1450 m). Small variations of surface elevation in the east-west direction are also present. Column water vapor amount usually decreases as the surface elevation increases, because atmospheric water vapor concentration decreases rapidly with altitude. Therefore, the column water vapor amount from the airport to Platteville was expected to increase. The dark-bright-dark-bright pattern from bottom to top in Fig. 2b indicates that real spatial variation, not related to the topographic effects, of water vapor distributions existed when the AVIRIS data were acquired. The observed spatial variation of column water vapor amount on the order of 0.1 cm or less indicates the high precision with which column water vapor amounts can be determined from AVIRIS data.

Precipitable water vapor fields, at a grid spacing of approximately 10 km, over the Rocky Mountain foothills extending roughly 300 km in both the east-west and the north-south directions were obtained from VAS data using a regression technique described by Birkenheuer (1991). Bias existed between PWV values obtained from the VAS data alone and the "true" PWV values. In order to remove the bias, PWV values obtained from VAS data alone were raised or lowered by a constant based on PWV values measured with microwave radiometers at the airport and at Platteville. The resulting bias corrected PWV field at 18:45 UTC 22 March (approximately one hour before the AVIRIS measurements) revealed a gradient structure in the Denver-Platteville area, which is similar to the gradient structure in Fig. 2b.

Figure 3 shows time series of PWV at (a) Platteville, (b) Denver, and (c) Elbert on 22-23 March 1990. Elbert is located approximately 60 km southeast of Denver. The continuous curves show 2-min time series from microwave radiometers. The rectangles are from the Cross-chain Loran-C Atmospheric Sounding System (CLASS) radiosondes. The squares are from the National Weather Service (NWS) radiosondes. The dark circles are from the VAS adjusted images, and the open circles from the AVIRIS measurements. The PWV values from AVIRIS and from the microwave radiometer measurements agreed to within 0.1 cm, but the relative difference is greater than 10%.

Because the PWV values from the microwave radiometer at Elbert were not used in the bias corrections discussed above, comparing PWV values from the VAS data with bias corrections to those from the Elbert microwave radiometer measurements is a blind test of the VAS PWV analysis technique. Fig. 3c shows that the VAS PWV analysis reported a consistently higher level of PWV over Elbert. A possible explanation for the discrepancy is presented below. The ground instantaneous field of view of VAS data is approximately 10 km. This large field of view would tend to blend the lower moisture level at the higher elevation terrain, where the microwave radiometer was located, with the higher moisture levels at adjacent lower elevation terrains, effectively raising the analyzed amount of PWV in a region like that of Elbert.

Fig. 3b shows that a PWV difference of 3 mm existed between the radiometer and the radiosonde data at 2300 UTC. This difference was due to the NWS balloon moving into a region of dry air, and did not reflect the build-up of moisture that was observed during this time by all three microwave radiometers. That a build-up was occurring was also supported by the two special CLASS radiosondes released at Elbert at 0000 and 0300 UTC 23 March. This increase in moisture was followed by a well-documented event of supercooled liquid water that lasted for three days (Stankov et al., 1990). The conclusion of the NWS balloon moving into a dry air region was based on the analyses (Gao et al., 1991) of wind profiles measured at the airport and of meteorological data from approximately 20 surface stations located in different parts of Colorado.

B. Death Valley, California

Death Valley is located in the southeastern part of California, near the Nevada border. AVIRIS data over the area were collected on September 29, 1989 during the Geologic Remote Sensing Field Experiment (GRSFE). Figure 4a shows an AVIRIS image (0.68 μm) of the site. The valley floor is located between the Trail Canyon alluvial fan (upper left corner) and the hills of Artists Drive (right side). One road in the upper part of the image traverses the valley floor. Another road located on the right portion of the image is nearly parallel to the valley floor. There are a number of geologic units within the AVIRIS scene (Hunt and Mabey, 1966). The valley floor consists of playa and salt units mixed with clay. The bright white areas are mostly pure salts. Fig. 4b shows a topographic map of the scene. The upper left corner of the image has an elevation of approximately 60 m. The highest portion of the Artists Drive hills has an elevation of approximately 240 m. The valley floor is very flat and below sea level, with elevations between approximately -85 and -73 m. The central portion of the valley floor is slightly lower in elevation than the western and the eastern portions of the valley floor. Also, the southern portion of the valley floor is slightly lower than the northern portion of the valley floor.

At the time of the AVIRIS overflight, some surface areas were wet. Reflectance spectra of samples collected from the field were made with the Geophysical and Environmental Research (GER) portable spectrometer. Curve 1 of Figure 5 shows a reflectance spectrum of a field sample collected over a wet spot within the bright white area in the upper part of Fig. 4a. The liquid water features near 0.98, 1.2, 1.6, and 2.2 μm are clearly seen. Curve 2 of Fig. 5 shows a spectrum obtained by ratioing an AVIRIS spectrum (Spec1) over the wet bright white area in the upper part of Fig. 4a against an AVIRIS spectrum (Spec2) over a drier area just left of the wet white area. The same set of liquid water features are also obvious. Curve 3 shows a spectrum obtained by ratioing the Spec2 against an AVIRIS spectrum (Spec3) over a higher hill area. Atmospheric water vapor features near 0.94 and 1.14 μm are seen. This indicates that the lower elevation valley floor has more water vapor than the hill areas.

The spectral curve fitting technique described by Gao and Goetz (1990) was used to derive simultaneously the atmospheric column water vapor amount and the equivalent liquid water thickness of the surface from the AVIRIS data. In this technique, the atmospheric water vapor transmittances were calculated with a narrow-band model and the liquid water transmittances were calculated using the liquid water absorption coefficients compiled by Palmer and Williams (1974). Fig. 6a shows the curve fitting of Spec1 by including only atmospheric water vapor absorptions in the fitting process. The fitted spectrum has larger values of reflectance than the observed spectrum near 1.2 μm. The overall fitting between the two spectra is poor. Fig. 6b shows the curve fitting by including both the water vapor and the liquid water absorptions in the fitting process. Significant improvement in the overall fit is achieved.

Figures 7a and 7b show the column water vapor image and the liquid water image derived from the AVIRIS data. The water vapor amounts over the hills are smaller than those over the valley floor. This is due to the decreasing atmospheric water vapor concentration with altitude. The slightly smaller water vapor amounts near the upper left corner of Fig. 7a than those over the nearby valley floor can also be attributed to the topographic effect. The liquid water image in Fig. 7b shows clearly the drainage patterns. Based on the topographic map of Fig. 4b, liquid water will flow from the hills on the right side and from the area near the upper left corner into the valley floor after rain. Also, because the southern portion of the valley floor has slightly lower elevations than the northern portion of the valley floor, the liquid water will further flow from top to bottom. A road traversing the valley in the upper part of Fig. 4a is slightly elevated and has acted as a dam, blocking the natural flow of water from the upper valley to the lower valley and causing more white salt to be deposited in areas north of the road. The long narrow drainage pattern (Fig. 7b) below the road indicates that the pipe beneath the road allows the water to flow from the northern to the southern portions of the valley floor. The liquid water thicknesses within the drainage patterns vary between approximately 0.04 and 0.46 cm. Areas having large amounts of white salt deposits tend to have larger liquid water thicknesses. This may be a true indication of the wetness of the salts. Field observations showed that the white salt areas are wetter than nearby areas not covered by the white salts. On the other hand, the solar radiation near 1 μm can penetrate deeper into the white salt than other materials. This can also effectively increase the liquid water thicknesses over the white salt areas.

By comparing Figures 7a and 7b, it can be seen that over the valley floor the areas with more liquid water seem to have more atmospheric water vapor. This is most evident over the two large areas having white salt deposits (one in the upper part of the scene and one in the lower part of the scene). Therefore, the spatial variation in atmospheric water vapor may be related to the evaporation of surface liquid water. The spatial variation of column water vapor amounts over the valley can not be attributed to the topography because the valley floor is

relatively flat with elevation differences of 12 m or less. In the future, we plan to make further studies of the correlations among water vapor, surface liquid water, topography, and mineralogy.

IV. Summary and Conclusions

We compared PWV soundings from the three separate remote sensing systems: Optical, VAS, and microwave radiometers. The microwave measurements were also compared with soundings from both NWS and CLASS radiosondes. The microwave and optical measurements agreed to within 1 mm, and the comparisons with the radiosondes were also either good or explainable. Gradient structures of water vapor are observed in both PWV images derived from AVIRIS and VAS data. Because of its large field of view, VAS has difficulties in resolving small scale features near sharp discontinuities caused by terrain. Each of the techniques can provide complementary information of PWV. The optical technique provides column water vapor amounts during clear conditions at a precision better than 1 mm and at high spatial resolution. The microwave radiometer provides nearly continuous data during both clear and cloudy conditions, but only at a limited set of locations. The column water vapor amounts derived from microwave radiometer data can be used to quantitatively adjust satellite PWV images provided by the VAS sounder (Birkenheuer, 1991). Because of the good horizontal resolution provided by the optical technique, optical soundings could provide significant insight into horizontal transport of water vapor. Such soundings could also be useful for GOES VAS verification.

The column water vapor amounts derived from AVIRIS data over Death Valley decrease with increasing surface elevation. The liquid water image shows surface drainage patterns. The spatial variations in atmospheric water vapor over the valley may be related to the evaporation of surface liquid water. The distribution of mineral deposits over the valley may also be related to the surface drainage patterns.

Atmospheric water vapor is a very complex, highly mobile species and we have a long way to go to fully understand and analyze this variable.

Acknowledgments

The authors are grateful to R. O. Green of the Jet Propulsion Laboratory for providing the AVIRIS spectral data. This work was partially supported by the Jet Propulsion Laboratory, California Institute of Technology under contract 958039 and the FAA under the contract DTAF01-90-Z-02005.

References

Alishouse, J. C., Total precipitable water and rainfall determinations from the Seasat Scanning multichannel microwave radiometer, *J. Geophys. Res.*, *88*, 1929-1935, 1983.

Birkenheuer, D. L., An algorithm for operational water vapor analyses integrating GOES and dual-channel microwave radiometer data on the local scale, *J. Appl. Meteor.*, (in press).

Chesters, D. C., L. W. Uccellini, and W. D. Robinson, Low-level water vapor fields from the VISSR Atmospheric Sounder (VAS) "split-window" channels, *J. Clim. Appl. Meteor.*, 22, 725-743, 1983.

Conel, J. E., R. O. Green, V. Carrere, J. S. Margolis, G. Vane, C. Bruegge, and R. Alley, Spectroscopic measurement of atmospheric water vapor and schemes for determination of evaporation from land and water surface using the Airborne Visible/Infrared Imaging Spectrometer (AVIRIS), *Proceedings of the IEEE Geosciences and Remote Sensing Society/USRI 1989 International Symposium*, 2658-2663, 1989.

Frouin, R., P.-Y. Deschamps, and P. Lecomte, Determination from space of atmospheric total water vapor amounts by differential absorption near 940 nm: Theory and airborne verification, *J. Appl. Meteorol.*, 29, 448-460, 1990.

Gao., B.-C., Ed. R. Westwater, B. B. Stankov, D. Birkenheuer, and A. F. H. Goetz, Comparison of column water vapor measurements using downward-looking optical and infrared imaging systems and upward-looking microwave radiometers, Submitted to *J. Appl. Meteor.* in April, 1991.

Gao, B.-C., and A. F. H. Goetz, "Column Atmospheric Water Vapor and Vegetation Liquid Water Retrievals From Airborne Imaging Spectrometer Data", *J. Geophys. Res.*, *95*, 3549-3564, 1990.

Goetz, A. F. H., G. Vane, J. Solomon, and B. N. Rock, Imaging spectrometry for Earth remote sensing, *Science*, *228*, 1147–1153, 1985.

Hogg, D. C., F. O. Guiraud, J. B. Snider, M. T. Decker, and E. R. Westwater, A steerable dual-channel microwave radiometer for measurement of water vapor and liquid in the troposphere, *J. Appl. Meteorol.*, *22*, 789–806, 1983.

Hunt, C. B., and D. R. Mabey, Stratigraphy and structure Death Valley, California, U. S. Geology Survey Professional Paper 494-A, 162 p., 1966.
Palmer, K. F., and D. Williams, Optical properties of water in the near infrared, *J. Opt. Soc. Am., 64*, 1107-1110, 1974.
Stankov, B. B., E. R. Westwater, J. B. Snider, and R. L. Weber, Remote sensor observations during WISP90: The use of microwave radiometers, RASS, and ceilometers for detection of aircraft icing conditions, NOAA Tech. Memo., ERL WPL-187, NOAA Wave Propagation Laboratory, Boulder, CO, 77pp., 1990.
Vane, G. (Ed.), Airborne visible/infrared imaging spectrometer (AVIRIS), *JPL Publ. 87-38*, Jet Propulsion Laboratory, Pasadena, Calif., 1987.
Westwater, Ed. R., and J. B. Snider, Applications of ground-based radiometric observations of millimeter wave radiation, *Alta Frequenza*. LVIII, 31-38, 1989.

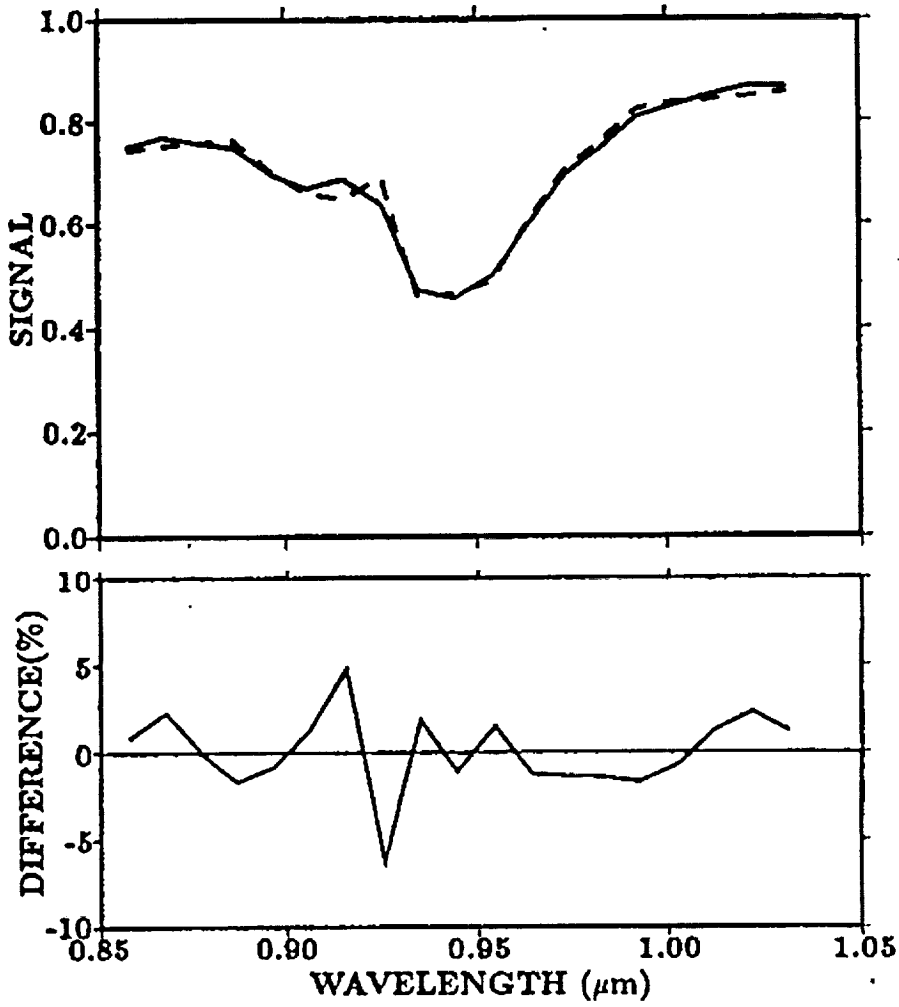

Fig. 1. An example of curve fitting of spectra. The top plot shows the observed spectrum (solid line) and the fitted spectrum (dashed line). The bottom plot shows the percentage differences between the observed and the fitted spectra.

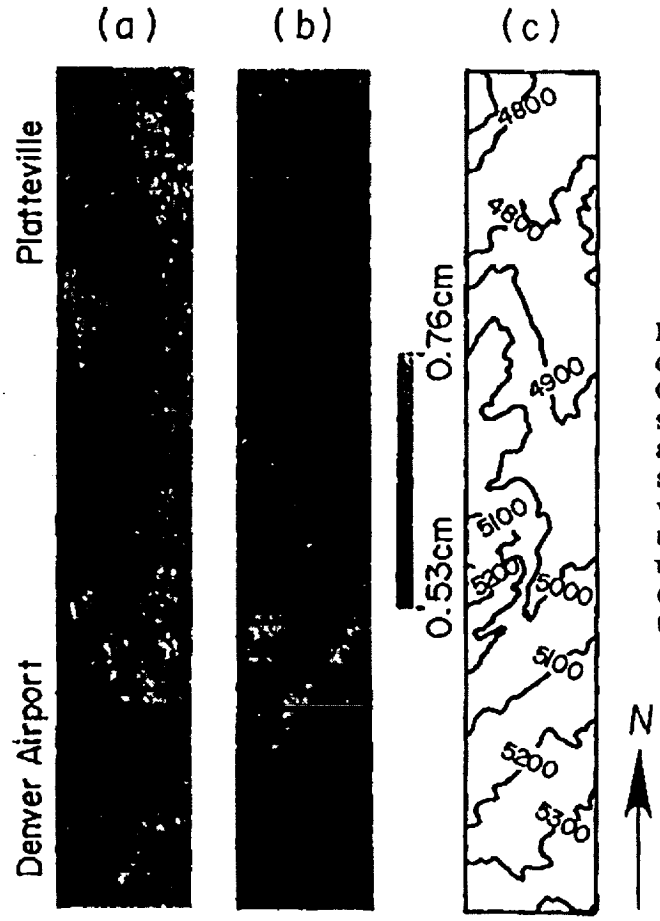

Fig. 2. Column water vapor retrievals from AVIRIS data measured over the Denver-Platteville area in Colorado on March 22, 1990. (a) An image of the scene processed from radiance of one channel centered at 0.86 μm, (b) a column water vapor image over the scene retrieved by curve fitting the 0.94-μm water vapor band absorption region, and (c) a topographic map of the scene. The elevations in the topographic map are in units of feet (1 foot = 30.48 cm). The distance from left to right side of the two images in this figure is approximately 11 km.

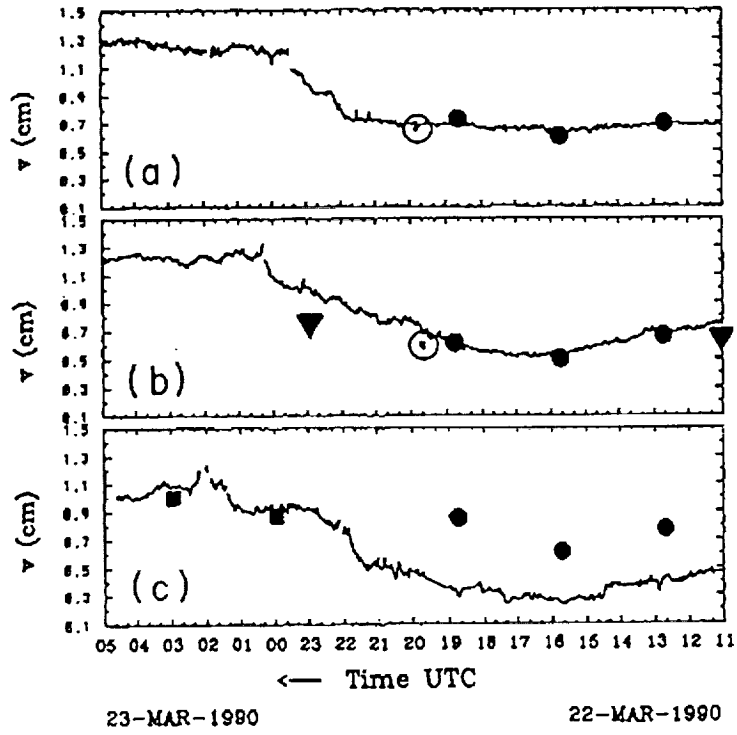

Fig. 3. Time series of precipitable water vapor at (a) Platteville, (b) Denver, and (c) Elbert on 22-23 March 1990. Continuous curves are from microwave radiometers, rectangles from CLASS radiosondes, squares from NWS radiosondes, dark circles from VAS-adjusted image, and open circles from AVIRIS.

(a)

(b)

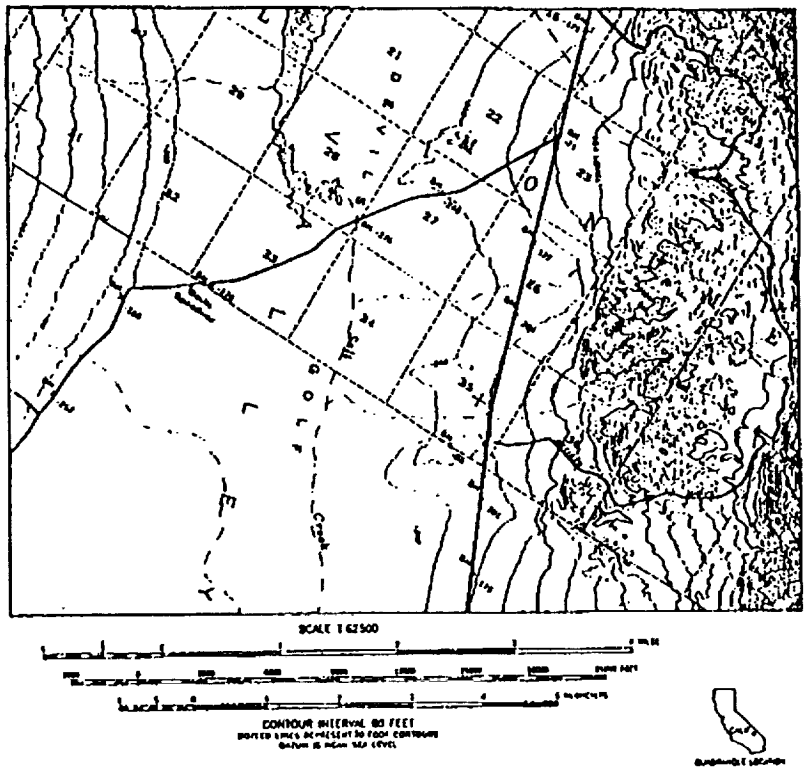

Fig. 4. (a) An image of Death Valley, California processed from radiance of one AVIRIS channel at 0.68 μm, and (b) a topographic map of the scene. The elevations in the topographic map are in units of feet (1 foot = 30.48 cm). The distance from left to right side of the image in this figure is approximately 12 km.

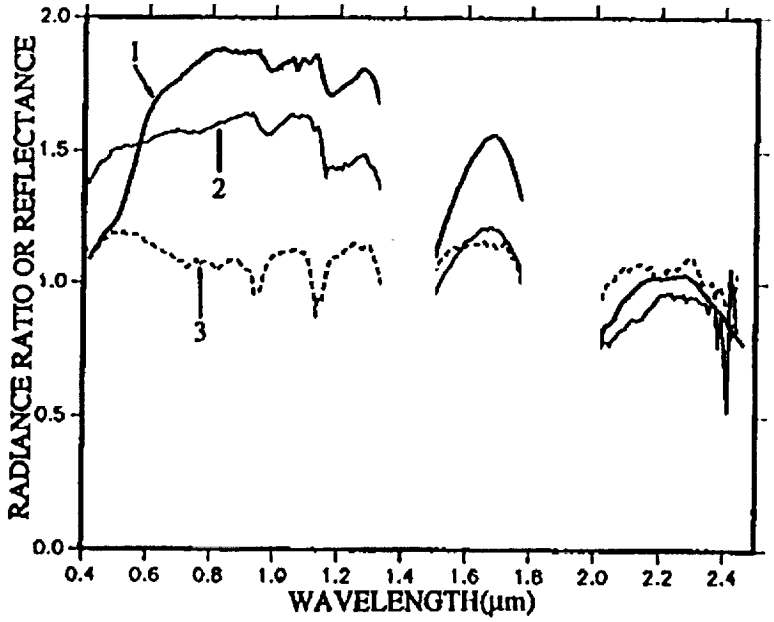

Fig. 5. A reflectance spectrum (multiplied by 5) of a wet sample collected from the field and two ratioed spectra from the AVIRIS data. See text for descriptions of the ratioed spectra.

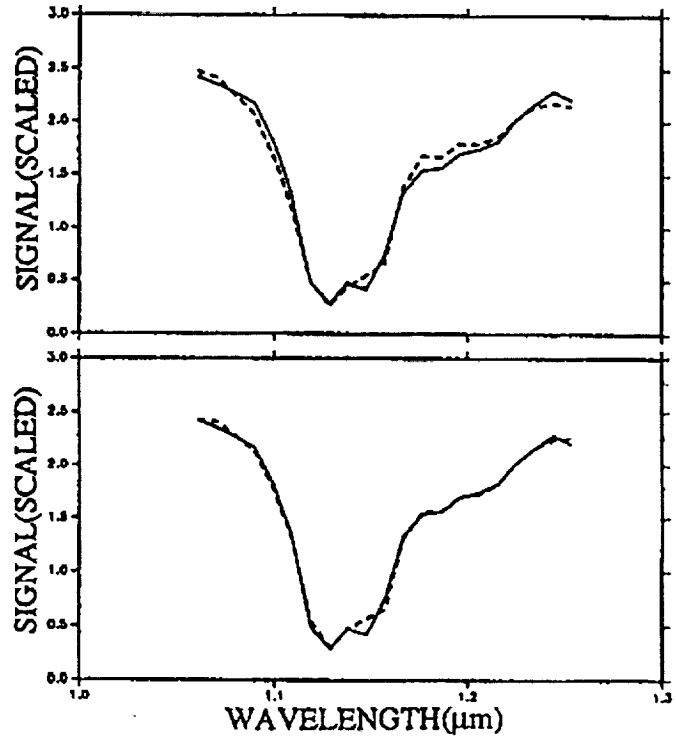

Fig. 6. Curve fitting of an AVIRIS spectrum over a bright, wet salt area. The top plot shows the observed spectrum (solid line) and the fitted spectrum (dashed line). Only the water vapor absorption is included in the fitting process. The bottom plot is similar to the top plot, except that both the water vapor and the liquid water absorptions are included in the fitting process.

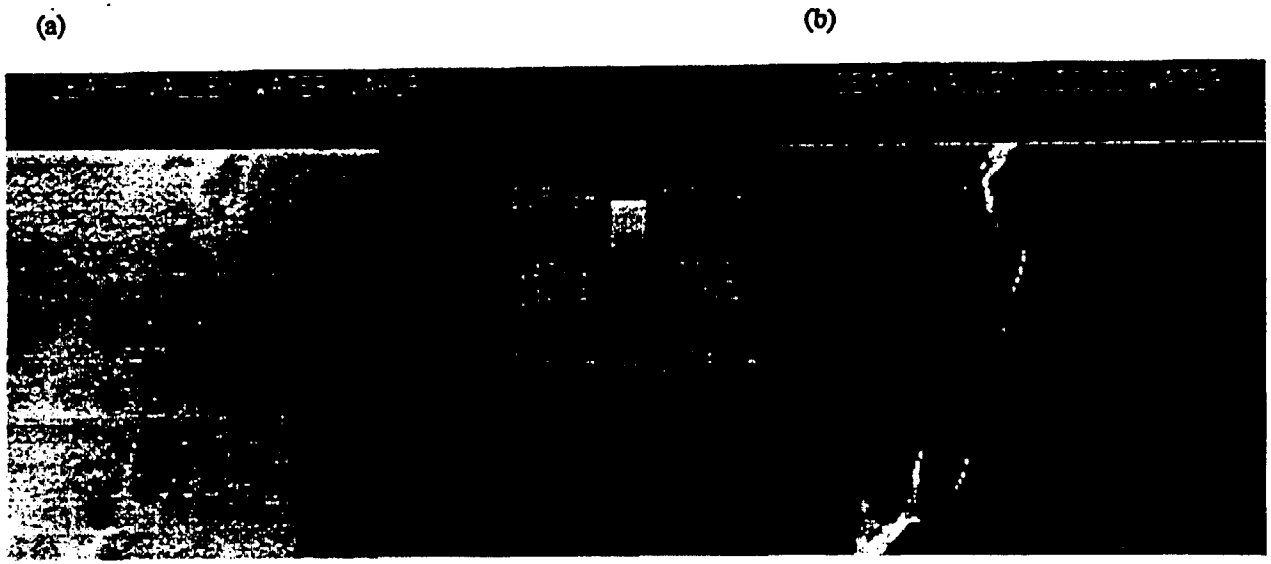

Fig. 7. Column water vapor image (a) and liquid water image (b) obtained from the AVIRIS over Death Valley.